Determining Circuit Model Parameters from Operation Data for PV System Degradation Analysis: PVPRO

Baojie Li[1], Todd Karin[1, 2], Bennet E. Meyers[3], Xin Chen[1], Dirk C. Jordan[4], Clifford W. Hansen[5], Bruce H. King[5], Michael G. Deceglie[4], Anubhav Jain[1]

1. Energy Technologies Area, Lawrence Berkeley National Laboratory, Berkeley, CA, USA
2. PV Evolution Labs (PVEL), Napa, CA, USA
3. SLAC National Accelerator Laboratory, Menlo Park, CA, USA
4. National Renewable Energy Laboratory, Golden, CO, USA
5. Sandia National Laboratories, Albuquerque, NM, USA

Abstract:

Physics-based circuit parameters like series and shunt resistance are essential to provide insights into the degradation status of photovoltaic (PV) arrays. However, calculating these parameters typically requires a full current-voltage characteristic (*I-V* curve), the acquisition of which involves specific measurement devices and costly methods. Thus, *I-V* curves of the PV system level are often not available. This paper proposes a methodology (PVPRO) to estimate these *I-V* curve parameters using only operation (string-level DC voltage and current) and weather data (irradiance and temperature). PVPRO first performs multi-stage data pre-processing to remove noisy data. Next, the time-series DC data are used to fit an equivalent circuit single-diode model (SDM) to estimate the circuit parameters by minimizing the differences between the measured and estimated values. In this way, the time evolutions of the SDM parameters are obtained. We evaluate PVPRO on synthetic datasets and find an excellent estimation of both SDM and the key *I-V* parameters (*e.g.*, open-circuit voltage, short-circuit current, maximum power, etc.) with an average relative error of 0.55%. The performance, especially the extracted degradation rate of parameters, is robust to various measurement noises and the presence of faults. In addition, PVPRO is applied to a 271kW PV field system. The relative error between the real and estimated operation voltage and current is <1%, suggesting that degradation trends are well captured. PVPRO represents a promising open-source tool to extract the time-series degradation trends of key PV parameters from routine operation data.

Keywords: Parameter estimation, single-diode model, degradation, photovoltaic, health monitoring

Nomenclature

DC	Direct current	P_{mp}	Maximum Power (W)
FF	Fill factor	V	Voltage (V)
G	Irradiance (W/m^2)	V_{mp}	Voltage at MPP (V)
I	Current (A)	V_{oc}	Open-circuit voltage (V)
I_o	Saturation current (A)	PV	Photovoltaic
I_{ph}	Photocurrent (A)	q	Electron's charge (C)
I_{mp}	Current at Maximum Power Point (A)	r^2	Coefficient of determination
I_{sc}	Short-circuit current (A)	RMSE	Rooted mean squared error
I-V curve	Current-voltage characteristic	R_s	Series resistance (Ω)
k_B	Boltzmann constant (J/K)	R_{sh}	Shunt resistance (Ω)
MPP	Maximum power point	sc-Si	Single crystalline silicon
n	Diode factor (unitless)	SDM	Single diode model
N_S	Number of cells of a PV module	STC	Standard test condition
		T_c	Cell temperature (°C)
		T_m	Module temperature (°C)

1 Introduction

In recent decades, the photovoltaic (PV) industry has experienced rapid growth worldwide, with installed solar capacity increasing by 19% in 2021 (SEIA, 2022). According to the 'Net Zero Emissions by 2050' scenario, solar electricity is expected to comprise 24.2% of global energy production (IEA, 2021). With the rapid developments in materials and designs, reliability issues are increasingly important (Zaghba et al., 2022; Zeb et al., 2022). Exposed to the harsh outdoor environment, PV systems are subject to various degradation mechanisms (Lillo-Sánchez et al., 2021; Mellit et al., 2018). Analyzing the degradation of the PV system is vital to predicting the system lifetime and accurately projecting project finances (Theristis et al., 2020). It is also essential to reveal the underlying mechanisms of the degradation, which may be caused by various factors like corrosion and defects (Asadpour et al., 2021; Asadpour and A. Alam, 2022). Understanding these degradation factors will greatly help in planning efficient operation & maintenance (O&M) (Rahman et al., 2021), preventing severe failures of PV systems (Alam et al., 2015) and feeding back to improve the next generation of systems.

Common degradation analysis strategies can be roughly split into remote monitoring and in-field measurements (Jordan and Kurtz, 2013). The remote strategies generally leverage operational data, like electrical and environmental factors, to perform the analysis (Jordan and Kurtz, 2014; Kumar and Kumar, 2017). Popular remote-monitoring strategies include the performance ratio method (Schardt and te Heesen, 2021), the reference yield method (Padmavathi and Daniel, 2013) and machine learning techniques (David et al., 2021; Mellit and Kalogirou, 2022). While these remote strategies permit real-time monitoring of PV systems, the available data is often limited. Comparatively, in-field strategies allow performing advanced measurements, like aerial IR imaging, *I-V* characterization (Li et al., 2021a), electroluminescence (EL) imaging (Chen et al., 2022; Jahn et al., 2018) and photoluminescence (PL) imaging (Doll et al., 2021; Vuković et al., 2022), which provide rich information to characterize the system status. Among the in-field techniques, *I-V* characterization extracts unique and valuable information about the health and performance of the PV array (Kalliojärvi-Viljakainen et al., 2022; Li et al., 2022). These include the electrical signatures (*e.g.*, open-circuit voltage V_{oc}, short-circuit current I_{sc}, fill factor FF) and the physics-based equivalent model parameters (*e.g.*, series resistance R_s and shunt resistance R_{sh}) (Li et al., 2021b; Wang et al., 2020). To extract the equivalent model parameters, various methods have been proposed in the literature, as reviewed in (Humada et al., 2020; Yang et al., 2020). Alternatively, instead of using *I-V* characterization, these model parameters can be estimated from information provided in the manufacturer datasheet (Batzelis, 2019). However, the actual model parameters are likely to degrade after years of operation (Ndiaye et al., 2013; Phinikarides et al., 2014). Therefore, the parameters extracted from the manufacturer datasheet generally do not represent the true model parameters. Comparatively, the parameters extracted from the *I-V* characteristics (*I-V* curves) measured in the field can reflect the true health condition of the PV system, thus allowing for accurate performance modeling (Humada et al., 2020), degradation analysis (Kumar and Kumar, 2017), as well as the quality assurance check of the PV system (De la Parra et al., 2017).

However, in-field *I-V* characterization is generally a time-consuming process, which requires site visits and specialized measurement devices (Pillai and Rajasekar, 2018). Additionally, *I-V* characterization with the most careful techniques still has noise uncertainty of 2-5% due to a variety of factors (Smirnov et al., 2010) (irradiance, spectral mismatch, temperature, etc.), making analysis of trends very difficult. With typical minimally-trained operators, the uncertainty of field *I-V* characterization is likely much higher. While continuous in-field single module *I-V* tracers are available (MorganSolar, 2022), these lead to additional cost and complexity for installation at the PV system level (Livera et al., 2019). Consequently, *I-V* curves of PV systems are often not available for the extraction of the electrical or equivalent circuit parameters for degradation analysis.

Given this fact, researchers have conceived alternative methods. Instead of using the entire *I-V* curves, partial curves (*i.e.*, a portion of the curve) or reduced *I-V* curve data (several key points) can also be leveraged to extract the model parameters. Both methods can effectively reduce the interference time caused by the measurement to the PV devices in operation. A common practice of partial curves is to use the data measured around the maximum power point (MPP). However, a key issue for this type of methodology lies in the determination of the optimal neighborhood range of MPP. For example, Cardenas et al. (Cardenas et al., 2017) utilize about 50% of the measurement (around the MPP) of an entire *I-V* curve. Lappalainen et al. (Lappalainen et al., 2020) select a portion of the *I-V* curve with voltage within ±3V of the MPP voltage (module open circuit voltage of 33 V) to fit the model. Kalliojärvi et al. (Kalliojärvi et al., 2022) statistically investigated the impact of the measurement range near MPP on the fitting performance of a single-diode model (SDM). It is shown that the portion of the curve where the corresponding power is above 50% of the MPP power provides a viable alternative to extract the model parameters. Concerning the reduced *I-V* curve data, the relevant research show difference in the selection of key points. A common strategy is to use the same parameters (like V_{oc}, I_{sc}, voltage at MPP V_{mp}, current at MPP I_{mp}) in the datasheet but measured in the field (Dobos, 2012), which then allows for the implementation of the same techniques (*i.e.*, parameter extraction form datasheet information) (Batzelis, 2019) to identify the model parameters. Besides, Tay et al. (Tay et al., 2017) proposed to use 6 points sparsely located on the *I-V* curve to estimate the model parameters. The Suns-Voc method (Killam et al., 2021; Wang et al., 2018) uses the V_{oc} to estimate diode parameters and reconstruct pseudo *I-V* curves. Toledo et al. (Toledo and Blanes, 2016) pick up 4 arbitrary points on the *I-V* curves to identify the SDM parameters. Most importantly, it should be noted that these methods, based on either partial or reduced *I-V* curve data, still require additional measurements other than the operation data (DC voltage and current), which will, therefore, inevitably affect the normal operation of the PV system but with reduced impact than the acquisition of entire *I-V* curves.

Since the operation data is the most common and readily available data for a PV system, some researchers have considered primarily using the operation data instead of the costly and time-consuming *I-V* characterization-based data to estimate the model parameters. Such methods have the advantage of requiring no additional measurements apart from the data already collected. Relying on operational and environmental data, Chakar et al. (Chakar et al., 2022) adopted the Teaching-Learning-Based Optimization technique to extract circuit parameters. Nevertheless, the training process is complicated, and the generalization capability is limited when applying the method to a new PV system. Based on a physical double-diode PV cell model, Sun et al. (Sun et al., 2019) introduced Sun-Vmp, an open-source method to extract the model parameters by fitting the physics-based circuit model using time-series maximum power point (MPP) data. This method is promising; however, in its current form, it relies on assumptions such as parameters following a monotonic degradation trend over time and could be improved in terms of fitting speed. In addition, the pre-processing procedure is simple without considering the operating and climatic conditions (like clear sky filters), which may deteriorate the performance when using noisy or impure field data.

Environmental measurements like irradiance and temperature are generally required for PV model parameter extraction. However, when these data are unavailable, some solutions may be applicable, in which parameter extraction can be performed without associated environmental data. For example, using *I-V* curves, the research (Lappalainen et al., 2022) presents a methodology to estimate both the model and environmental parameters via SDM fitting. The identified irradiance and temperature exhibit high accuracy even during sharp transitions and low irradiance conditions. Similar research is performed by (Jones and Hansen, 2019), where an algorithm is proposed to identify model parameters from individual *I-V* curves.

In this manuscript, we propose a novel methodology (PVPRO) to extract the PV model parameters for degradation analysis. Notably, PVPRO only requires routine operational and environmental data; these are commonly available measurements for modern PV systems (Lindig et al., 2020), and additional measurements of entire, partial, or reduced *I-V* curve data are not required. Compared to past methods that also rely on operational data, PV-Pro does not assume a monotonic degradation trend of parameters as in (Sun et al., 2019) but introduces more comprehensive pre-processing techniques to handle noisy data. Compared to the machine learning approach in (Chakar et al., 2022), PV-Pro does not require retraining the model for new PV systems, which substantially improves the transferability and usability of the application.

The contribution of this paper is reflected in the following aspects: 1) A comprehensive methodology for parameter estimation and degradation analysis based on easily accessible PV operation and environmental data and requiring no additional measurements is proposed; 2) Time evolution trends of the model and *I-V* curve parameters are shown to be well captured on synthetic data sets; 3) The methodology is robust to measurement interference and the presence of faults; 4) An open-source Python package is available to perform the analysis (https://github.com/DuraMAT/pvpro).

The remainder of this paper is organized as follows: Section 2 presents the methodology of PVPRO, including the preprocessing and parameter estimation. Section 3 evaluates PVPRO using synthetic datasets under three case studies. A demonstration of PVPRO on a field PV dataset is given in Section 4. Discussions on the parameter estimation and the challenges are presented in Section 5. Section 6 concludes the paper.

2 Methodology of PVPRO

The main concept of PVPRO is to use operation data (DC current I_{DC}, DC voltage V_{DC}, module temperature T_m, and plane-of-array irradiance G) to determine the time-evolution of PV array SDM parameters at standard test conditions (STC, $G = 1000W/m^2$, $T_m = 25°\text{C}$), as depicted in Fig. 1. Specifically, the analysis pipeline of PVPRO consists of 2 steps, namely the preprocessing of data and the parameter estimation, which are described below in Section 2.1 and 2.2, respectively.

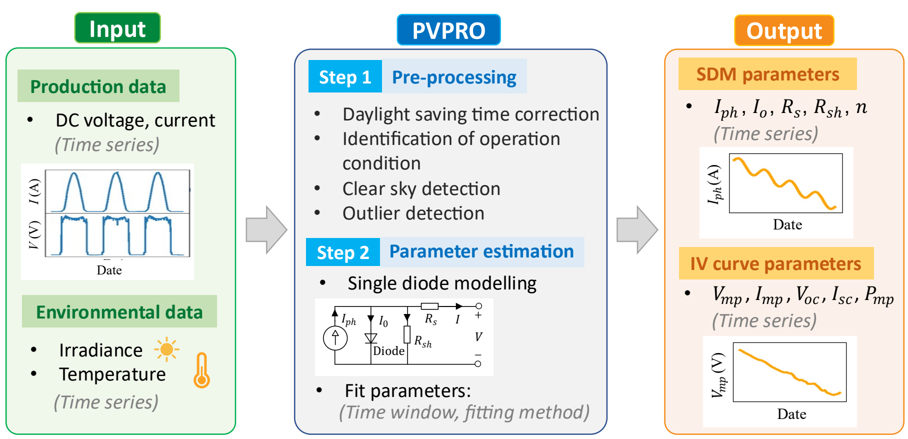

Fig. 1 Flowchart illustrating PVPRO analysis. The overall goal of PVPRO is to estimate SDM parameters and *I-V* curve parameters using only typical production and environmental data as inputs.

2.1 Pre-processing of data

Field-measured PV data is subject to noise and may contain erroneous values, therefore it is essential to perform efficient pre-processing of the raw data. To this end, PVPRO applies the following operations: 1) remove the daylight-saving time discontinuities (if present); 2) identify the operation condition to filter data at periods of inverter clipping and off-MPP operations; 3) detect clear sky periods; 4) detect and remove the outliers.

2.1.1 Daylight saving time correction

When the measurement of field data contains DST shifts, PVPRO adopts the DST correction function provided in the Solar data tools (Meyers et al., 2022, 2020) to correct the data timestamp to eliminate the shifts.

2.1.2 Identification of operation condition

The PVPRO algorithm is principally designed for data at maximum power point (MPP). However, it is not typically reported whether an inverter is at MPP or other operating points (open circuit, clipped, *etc.*). To better select the data for analysis, PVPRO identifies the operating condition of the PV array based on the electrical output and environmental data. The operating condition can be: operating at MPP, inverter off, open-circuited, clipped, or anomaly. The detailed procedure is provided in Supplementary Information (SI) Section A). This step allows users to decide which type of data to use for the following analysis. In this research, only MPP data points are included in the data set PVPRO analysis. An example is illustrated in Fig. 2 using a public PV dataset (NIST ground array) from 2015 to 2019 (Boyd et al., 2017).

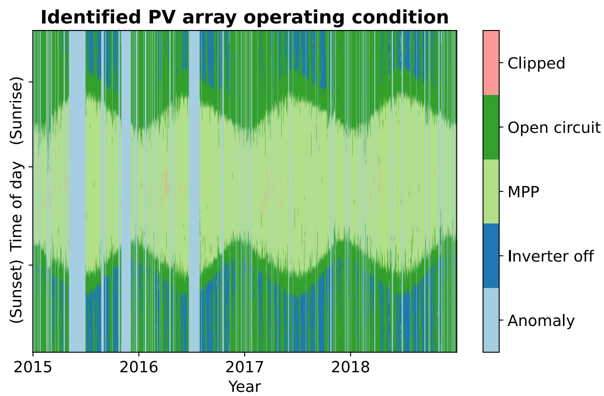

Fig. 2 Example of automatically identified operating conditions of the preprocessing routine using data of the NIST ground array from 2015 to 2019. Five PV array conditions are considered and labeled by different colors. The y-axis presents the time of day with the approximate sunrise and sunset time marked. It is observed that the PV array is generally under MPP condition during the daytime.

2.1.3 Clear time detection

Rapid changes in irradiance can lead to higher errors in the predicted operation point due to the spatial difference from the irradiance sensor to the array and imperfect synchronization between the irradiance/temperature sensors and the PV array (Modbus protocol typically has 30 seconds to minutes between acquisitions on each different sensor) (Friesen et al., 2018). To reduce the impact of fast weather changes on the extracted parameters, the data set is filtered to include only clear sky conditions. We accomplish this with an efficient clear time detection algorithm – statistical clear sky fitting (SCSF) algorithm (provided in Solar data tools (Meyers et al., 2020)) is employed with an example plotted in Fig. 3. Compared to other clear sky algorithms (Alia-Martinez et al., 2016; Ineichen, 2016), SCSF is independent of traditional atmospheric and geometric modeling techniques and resilient to shading conditions (Meyers et al., 2019). SCSF also minimizes the effects of spectral changes which are not accounted for otherwise. From Fig. 3, it is observed that on cloudy days, the clear sky time (marked in red points) could be well identified for analysis.

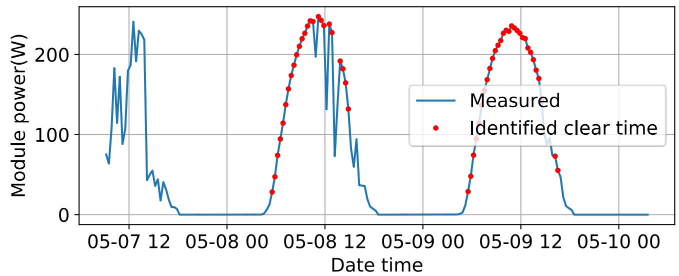

Fig. 3 Example of identified clear time based on module output power. On cloudy days, the SCSF algorithm correctly identifies the clear periods, marked in red points.

2.1.4 Outlier detection and removal

For field PV data, outliers are commonly encountered due to various reasons, such as non-synchronous measurements, clouds, signal noise, and sensor issues (Li et al., 2020). It is thus essential to carefully identify and remove such outliers. Generally, the measured I_{DC} is expected to be approximately proportional to the irradiance G and V_{DC} is linearly related to module temperature T_m. Accordingly, we identify such outliers by performing a linear regression of I_{DC} as a function of G and V_{DC} by T_m. The Huber regressor (Sun et al., 2020), which minimizes the squared differences and is robust to outliers in the fitting procedure. A threshold parameter (default value of 2) can be adjusted by the user based on the number of data points to determine the boundary between outliers and retained points (Sun et al., 2020). An example application for the detection of current and voltage outliers is shown in Fig. 4 using the NIST ground array dataset.

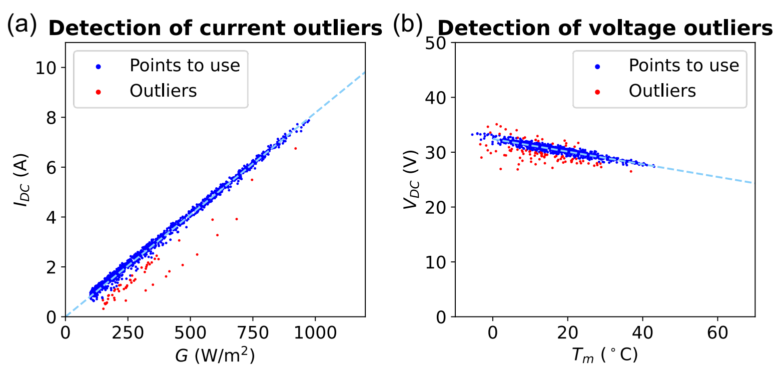

Fig. 4 Example of detected outliers and points to retain for analysis. (a) Detection of I_{DC} outliers as a function of G. (b) Detection of V_{DC} outliers as a function of T_mParameter estimation.

2.2 Parameter estimation

After pre-processing the data by performing the four operations presented in Section 2.1, PVPRO performs the SDM parameter estimation, with the procedure outlined in Fig. 5. The single-diode model (SDM) is adopted as the equivalent circuit model in this research, which is simple but can sufficiently characterize the performance of PV modules (Humada et al., 2016) in most situations and is also suitable for the case of changing environmental conditions (de Blas et al., 2002). Notably, PVPRO processes the time-series operation and environmental data by splitting the data into time windows. The evolution trend of the SDM parameters is obtained by concatenating the estimated results from each time-window data. Details of each step of the parameter estimation procedure are described next.

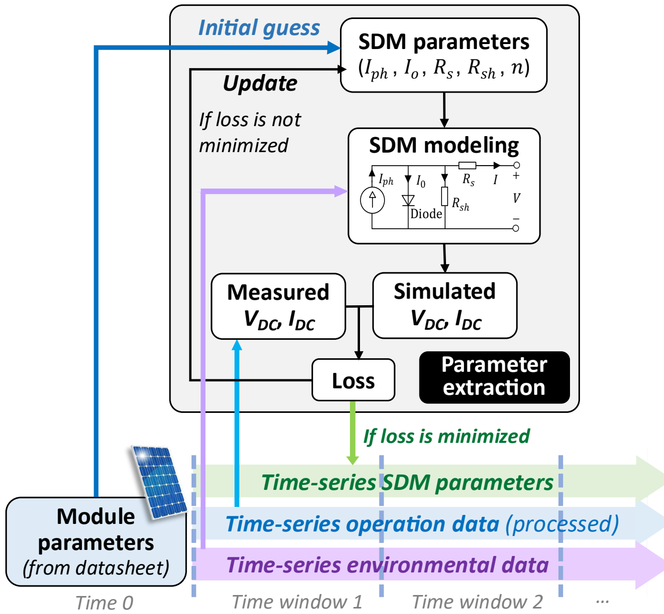

Fig. 5 Flowchart illustrating the estimation of SDM parameters using PVPRO. The whole process is performed on the time-series processed operation and environmental data. First, the initial guess of the SDM parameters is estimated from the module parameters. Then, for each time-window data, based on the SDM modeling, the V_{DC} and I_{DC} are estimated at the measured environmental conditions. These are compared with the measured values to compute a loss value. The SDM parameters are repeatedly updated until the loss is minimized, which marks the completion of the parameter extraction for that time-window data. This process is applied to all the time windows. In this way, PVPRO finally outputs a time series of SDM parameters.

2.2.1 Initial estimation of model parameters

The first step of the fitting procedure is to perform an initial guess of the SDM parameters of the PV module from the manufacturing datasheet. The single diode equation (1) includes five primary parameters, *i.e.*, the photocurrent (I_{ph}), saturation current (I_o), series resistance (R_s), shunt resistance (R_{sh}), and the diode factor (n). These parameters under different irradiance (*G*) and cell temperature (T_c) are expressed from (2) to (5) based on the values at the reference condition (I_{ph_ref}, I_{0_ref}, R_{sh_ref}, R_{s_ref}, n_{ref}) using the De Soto model (De Soto et al., 2006). The initial guess of the five SDM parameters at the reference condition is obtained from the module datasheet information using the 'pvlib.ivtools.sdm.fit_desoto' function (Holmgren et al., 2018), which obtains the reference parameters by optimizing the De Soto model functions (De Soto et al., 2006). R_s and n are assumed constant at its reference value, *i.e.*, R_{s_ref} and n_{ref} (De Soto et al., 2006). T_c is estimated from the module temperature (T_m) using the Sandia Array Performance Model provided in pvlib (Holmgren et al., 2018). Note that the R_{sh} in the DeSoto model is proportional to the inverse irradiance. This assumption presents problems in the parameter extraction, for example, R_{sh} could become unbounded as irradiance falls to 0. Therefore, we add a constant (G_{sh_extra}) as indicated in (1). This modified DeSoto model is then leveraged to extract the five SDM parameters, which are adopted as the initial parameters for PVPRO analysis.

$$I = I_{ph} - I_0\left[\exp\left(\frac{V+IR_s}{nN_s k_B T/q}\right) - 1\right] - (V + IR_s)\left(\frac{1}{R_{sh}} + G_{sh\_extra}\right) \quad (1)$$

$$I_{ph} = \frac{G}{G_{ref}}\left[I_{ph\_ref} + \alpha_{I_{sc}}\left(T_c - T_{c\_ref}\right)\right] \quad (2)$$

$$I_0 = I_{0\_ref}\left[\frac{T_c}{T_{c\_ref}}\right]^3 \exp\left[\frac{1}{k}\left(\frac{E_{g\_ref}}{T_{c\_ref}} - \frac{E_g}{T_c}\right)\right] \quad (3)$$

$$E_g = E_{g\_ref}\left[1 - dE_g dT\left(T_c - T_{c\_ref}\right)\right] \quad (4)$$

$$R_{sh} = R_{sh\_\,ref}\frac{G_{ref}}{G} \quad (5)$$

where,

- N_S: Number of cells connected in series of a PV module
- k_B : Boltzmann constant (1.38×10^{-23} J/K)
- q: Electron's charge (1.6×10^{-19} C)
- I_{0_ref}: Reference value of I_o at STC
- I_{ph_ref}: Reference value of I_{ph} at STC
- R_{sh_ref}: Reference value of R_{sh} at STC
- E_g: Material bandgap
- $dE_g dT$: temperature coefficient of bandgap energy, depends on the PV technology

Based on the initial parameters, the SDM could predict the per-module maximum power point under any environmental conditions. An illustration of the estimated module V_{mp} and I_{mp} using the environmental data from the NIST ground array dataset is presented in Fig. 6, where the estimated V_{DC} and I_{DC} are compared with the measured ones.

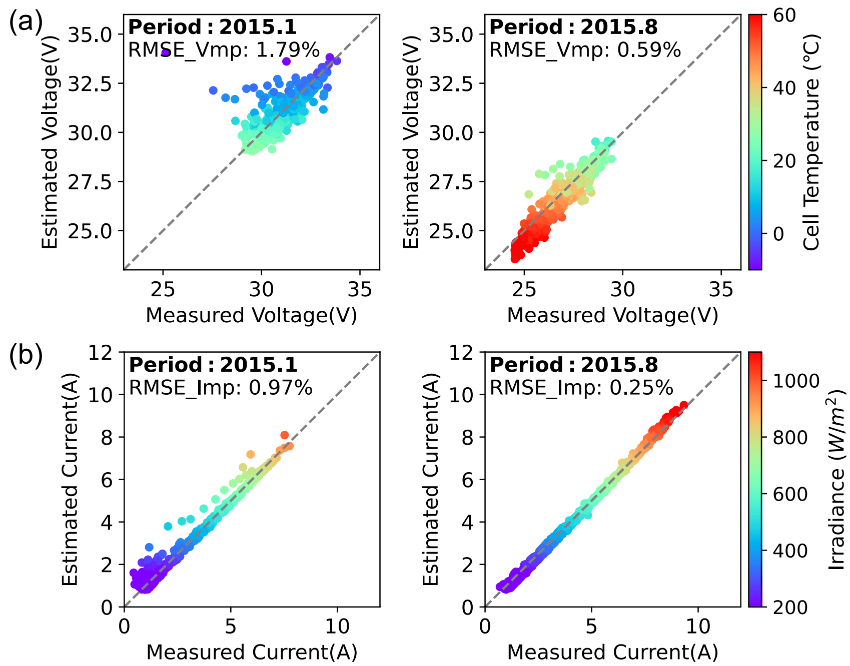

Fig. 6 Measured and estimated V_{DC} and I_{DC} (using the SDM with initially estimated parameters) at 2 periods, i.e., January and August in 2015 (a): V_{DC} (b): I_{DC}. We can observe that for the initially estimated parameters, the fit quality varies under different periods. Refinements to the SDM parameters are thus conducted by PVPRO as discussed in the context.

To quantify the accuracy of the SDM with the initial parameters, the root mean squared error (RMSE) between the estimated and measured values for V_{DC} and I_{DC} is calculated. From the results, the RMSE varies when using different periods of data (like in different seasons), as shown in Fig. 6. This indicates that the SDM with the initial parameters does not fit all the periods of measured data. In addition, the parameters may also change over time due to degradation. Thus, the SDM parameters need to be determined dynamically based on the data of each time period, which is the task of the next step.

2.2.2 Fitting of model parameters

As presented in Fig. 5, to fit the SDM parameters, a loss needs to be computed to quantify the difference between the estimated and measured V_{DC} and I_{DC}. Here, the L2 loss is adopted, which is stable and enables a fast convergence (Allen-Zhu et al., 2018). To help ensure an equal weight of V_{DC} and I_{DC}, both losses are divided by the median value as presented in (6). The mean value of the L2 loss of V_{DC} and I_{DC} across all measurement points is adopted as the total loss.

$$L2\_Loss = \left[\left(\frac{V_{DC}^{modeled} - V_{DC}^{measured}}{V_{DC}^{median}}\right)^2 + \left(\frac{I_{DC}^{modeled} - I_{DC}^{measured}}{I_{DC}^{median}}\right)^2\right]/2 \quad (6)$$

Next, the fitting procedure is performed. L-BFGS-B (Liu and Nocedal, 1989) is adopted as the solver, which permits a good optimization performance while using a limited amount of computer memory. The solver updates the SDM parameters in each loop. The fitting process is marked complete when the loss is minimized, or the maximum iterations are reached. The number of the maximum iterations is set to 500, which allows a good compromise between fitting performance and speed. Considering the significant variance in the order of magnitude of the five parameters (I_0 is usually in the range [10^{-10}A, 10^{-7}A] while R_s in [0Ω, 3Ω]), the numerical value of the five SDM parameters are normalized to fall within similar ranges to improve the numerical performance of the fitting algorithm (the specific numerical transformation functions are listed in Section B of the SI). Lower and upper bounds are recommended for the SDM parameters which permit the estimated values to fall into reasonable ranges. Details of the setup of bounds are provided in Section C of the SI.

Assuming that the model parameters are relatively stable within a short period, the data is split into time windows to perform the fitting procedure as shown in Fig. 5. The length of the time window can be adjusted depending on the time length of the data to process. When dealing with years of data, our default recommendation is to set the time interval as 2 weeks (14 days), which permits enough data points per iteration and maintains good time resolution. Using this fitting procedure, PVPRO can then estimate the time evolution of the SDM parameters based on the PV operation and environmental data.

3 Performance evaluation using synthetic datasets

PVPRO is first evaluated on synthetic datasets, which are generated based on controlled environmental data and SDM parameters, as illustrated in Fig. 7. Using such synthetic datasets, the performance of PVPRO can be quantified by comparing the estimated SDM parameters with the ground truth. Notably, synthetic measurement noise can be added to the measurement and the SDM parameters can be configured to demonstrate a specific time-based pattern (like with the presence of fault or steady degradation). Accordingly, this section will present 3 case studies: Section 3.1 demonstrates PVPRO using a synthetic dataset modelling a 11kW PV array. Section 3.2 investigates the impact of the measurement error (random and systematic error (Dirnberger and Kraling, 2013; Reise et al., 2018)) on the performance. Section 3.3 evaluates PVPRO in the presence of faults.

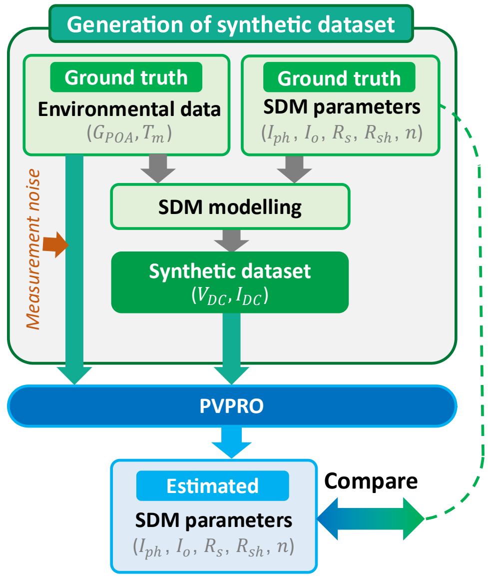

Fig. 7 Diagram illustrating testing of PV-Pro on synthetic datasets. First, a synthetic dataset is generated based on a chosen ground truth pattern for both SDM parameters and environmental data. Next, the SDM simulates the operation data, and noise can be added to the environmental data. PVPRO is provided with these environmental and operation data but without the SDM parameters. Instead, the SDM parameters will be estimated by PVPRO and are compared with the ground truth.

3.1 Case study using a synthetic dataset modeling an 11kW PV array

Based on the flowchart in Fig. 7, a synthetic dataset is generated for an 11kW PV array of 50 single crystalline silicon (sc-Si) modules. The true (generated) initial SDM parameters and corresponding *I-V* parameters are listed in Table 1. The array consists of 5 strings with 10 modules connected in series in each string. The environmental parameters are taken from 4 years (1998-2002) of meteorological data – NSRDB database (version 3.0.1) (Sengupta et al., 2018) at 37° 53' 24"N 122° 15' 36"W, which provides the true values of the plane-of array irradiance (G_{POA}), ambient temperature (T_a), wind speed, etc. The module backsheet temperature (T_m) is determined from the G_{POA}, T_a and wind speed using the common temperature translation method (D.L. King et al., 2004). Measurement noise is not included in this case study (the impact of the noise will be systematically studied in Section 3.2).

Table 1 Module parameters (*I-V* and SDM parameters)

***I-V* parameters**	**Value**	**SDM parameters**	**Value**
V_{mp_ref}	38.3 V	I_{ph_ref}	6.0 A
I_{mp_ref}	5.65 A	I_{o_ref}	1E-10 A
V_{oc_ref}	45.89 V	n_{ref}	1.2
I_{sc_ref}	6.0 A	R_{s_ref}	0.35 Ω
P_{mp_ref}	216 W	R_{sh_ref}	600 Ω

3.1.1 Determination of the degradation pattern for the synthetic dataset

To approximate the field-measured long-term PV operation data, degradation over time is artificially introduced to the SDM parameters (I_{ph_ref}, I_{o_ref}, R_{s_ref}, and R_{sh_ref}) to generate the synthetic dataset. The diode factor n_{ref} is assumed constant. The increase of R_{s_ref} and the decrease of R_{sh_ref} are intended to simulate corrosion and degradation of solder bonds (Aghaei et al., 2022). Specifically, a linear degradation is set for R_{s_ref} (0.02 Ω/year, 5.71%/year), R_{sh_ref} (-10 Ω/year, 1.67%/year), and

I_{0_ref} ($1e^{-11}$ A/year, 10%/year) along with a degradation with seasonal variation for I_{ph_ref} (linear degradation 0.05 A/year, -0.83%/year, the seasonal amplitude of 0.025A). The decrease of I_{ph_ref} reflects the degradation of I_{sc_ref} while the I_{0_ref} for V_{oc_ref}. The degradation rates are chosen by considering both the module parameters and the common rates reported in the literature which are obtained from long-term field tests (Kahoul et al., 2021).

3.1.2 Estimation results

Given the synthetic dataset, PVPRO outputs the estimated SDM parameters (I_{ph_ref}, I_{o_ref}, R_{s_ref}, R_{sh_ref}, n_{ref}) at the reference condition, i.e., STC in this research. Then, using these parameters, the SDM could predict the estimated *I-V* parameters at the reference condition (V_{mp_ref}, I_{mp_ref}, V_{oc_ref}, I_{sc_ref}, P_{mp_ref}). For this analysis, PVPRO fit parameters are set to values listed in SI Table S3. The ground truth of the *I-V* parameters is extracted from the *I-V* curves modeled by the SDM, as depicted in Fig. 7. The relative root-mean-square error (RMSE) and the coefficient of determination (r^2 score) are adopted as the evaluation metrics (detailed in Section E of SI). The relative RMSE quantifies the average error of estimation, while the r^2 score reflects the matching degree of the degradation trend of the parameters. The estimated *I-V* and SDM parameters with the ground truth are presented in Fig. 8, where the year-of-year (YOY) trends are also highlighted. The estimated and true degradation rate of these parameters are summarized in Table 2.

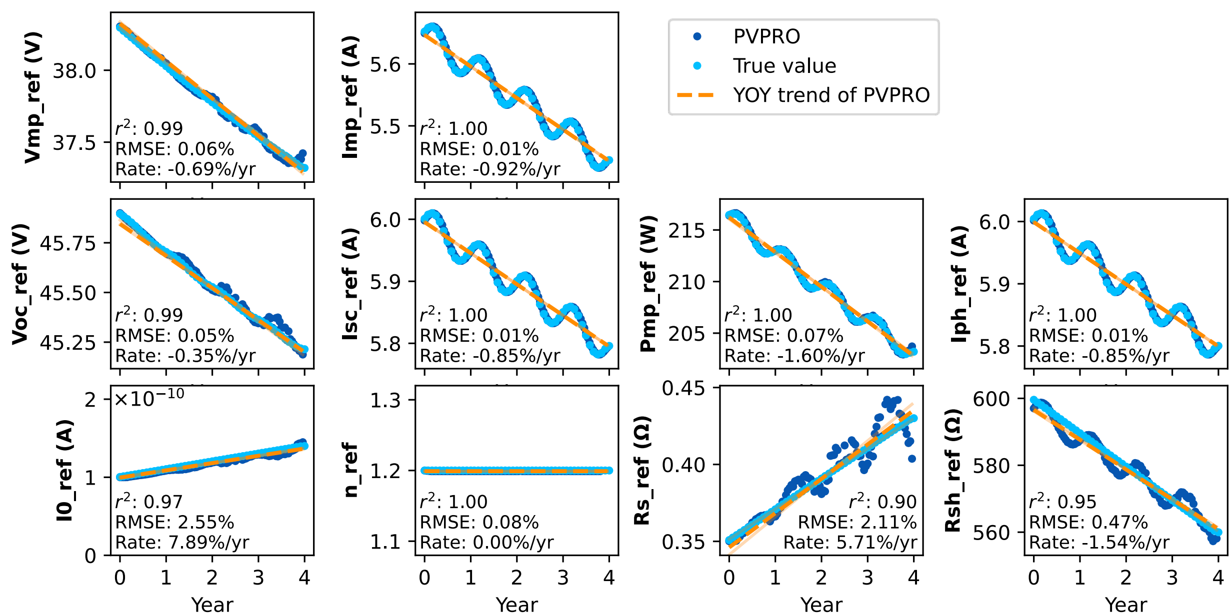

Fig. 8 Degradation trend of *I-V* and SDM parameters estimated by PVPRO (the dashed line represents the fitted YOY trend of parameters). Overall, PVPRO achieves good estimation of the parameters with r^2 score>=0.90.

Table 2 Degradation rates of estimated *I-V* and SDM parameters

		Estimated degradation rate (%)	**Reference degradation rate (%)**	**Relative rate error (%)**
***I-V* parameters**	V_{mp_ref}	-0.69	-0.64	7.37
	I_{mp_ref}	-0.92	-0.947	3.22
	V_{oc_ref}	-0.35	-0.37	4.23
	I_{sc_ref}	-0.85	-0.88	3.71
	P_{mp_ref}	-1.60	-1.564	2.41
	Mean±std	**-0.88±0.41**	**-0.88±0.44**	**4.18±1.70**
	I_{ph_ref}	-0.85	-0.879	3.81

SDM parameters	I_{o_ref}	7.89	9.95	20.70
	n_{ref}	0.0	0.0	-
	R_{s_ref}	5.71	5.71	0.05
	R_{sh_ref}	-1.54	-1.66	7.68
	Mean±std	**2.80±4.08**	**3.28±5.54**	**8.06±7.78**

At first glance at the extracted evolution trend, it is observed that the pre-determined periodic wave of I_{ph_ref} (conceived to approximate seasonal variation) also propagates into the current-related *I-V* curve parameters (I_{mp_ref}, I_{sc_ref}, and P_{mp_ref}). For other parameters, an overall linear evolution trend is exhibited. As for the performance, for all the parameters, PVPRO achieves an excellent estimation with the average relative RMSE 0.55% and the r^2 score of 0.98. For the *I-V* parameters (V_{mp_ref}, I_{mp_ref}, V_{oc_ref}, I_{sc_ref}, P_{mp_ref}), the performance of PVPRO is even better, with the r^2 score reaching nearly 1 and relative RMSE less than 0.1%. The average relative error of degradation rate is also below 5%, as presented in Table 2. It should be noted that V_{mp} and I_{mp} under various irradiance and temperatures are used to minimize the loss (as introduced in Fig. 5). Thus, it is logical to achieve a good performance of V_{mp_ref} and I_{mp_ref} under reference condition (i.e., STC) as these are the parameters for which loss is minimized. Note that, V_{oc_ref}, I_{sc_ref} and P_{mp_ref} are the parameters estimated by the SDM, which are indirectly optimized using V_{mp} and I_{mp}. Their high accuracy, consequently, demonstrate the capability of PVPRO for the estimation of the *I-V* parameters through the SDM modeling.

Regarding the SDM parameters, the overall estimation accuracy is lower than the *I-V* parameters with the average RMSE of 1.04% and degradation rate error of 8.06%. Comparatively, I_{ph_ref}, I_{o_ref}, and n_{ref} matched well the evolution trend of the true values. It may be noted that the estimated I_{o_ref} has a relatively large relative RMSE (2.55%) and degradation rate error (20.70%). This is due to the small value of I_{o_ref}, which is around 10^{-10} A. For the estimated R_{s_ref} and R_{sh_ref}, the seasonality variation is also observed, especially for R_s, which leads to the high RMSE and degradation rate error as the true degradation trend is linear. Nevertheless, the r^2 score for all the parameters is good, equal to or higher than 0.90. Thus, in the absence of measurement noise, we thereby conclude that PVPRO performs very well for capturing degradation trends.

3.2 Impact of random and systematic measurement noise

The results presented above are from a dataset free of additional measurement noise. To evaluate the robustness of PVPRO when dealing with different data quality, we study the effect of two measurement errors to G and T_m: (i) random noise and (ii) systematic errors. The random noise is set to a Gaussian distribution sampled independently at each point. The systematic error is set to a constant bias to the measurement values, which is generally due to the calibration error or measurement offset (Reise et al., 2018). We vary the noise level of these two types of noise and examine the corresponding average estimation error (relative RMSE, r^2 score, and degradation rate error) of the *I-V* (V_{mp_ref}, I_{mp_ref}, V_{oc_ref}, I_{sc_ref}, P_{mp_ref}) and SDM (I_{ph_ref}, I_{o_ref}, R_{s_ref}, R_{sh_ref}, n_{ref}) parameters are shown in Fig. 9 and Fig. 10. The details on the estimation error of each parameter are given in Section F of the SI.

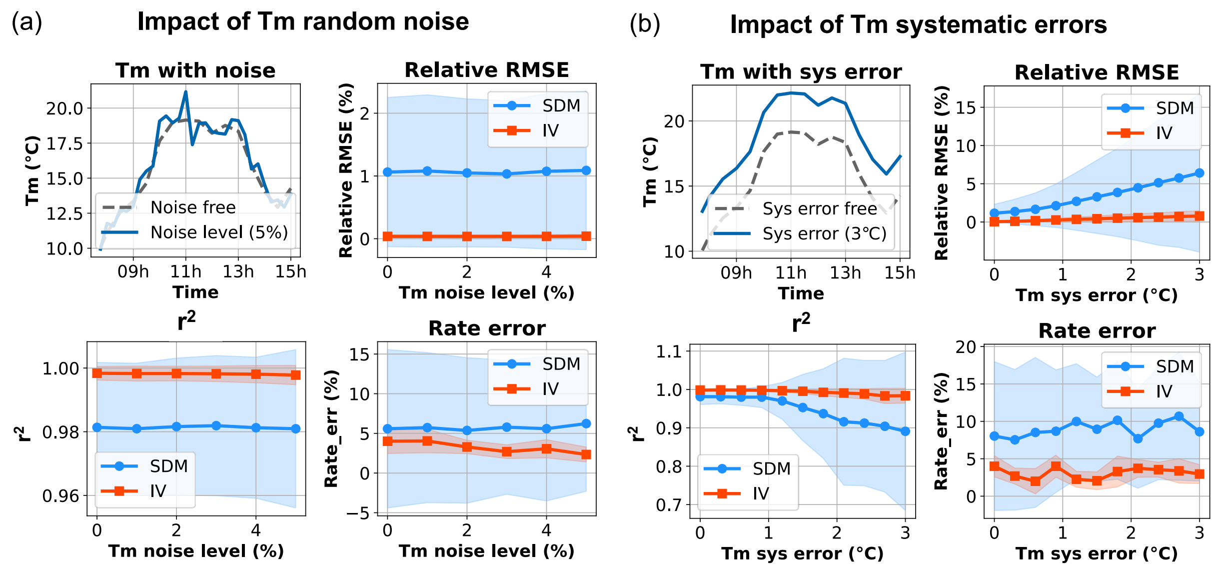

Fig. 9 (a) Example of module temperature (Tm) with random noise and the three metrics of estimated SDM and *I-V* parameters with Tm under different random noise levels. The noise level refers to the variance of the normal distribution added to the Tm. (b) Example of Tm with systematic error introduced and the three metrics of estimated SDM and *I-V* parameters with Tm under different systematic error levels. The dotted lines refer to the mean value of all the five SDM or five *I-V* parameter errors, while the filled area outlines the standard deviation of the parameter errors.

For Fig. 9, it is apparent that *I-V* parameters are better estimated than SDM parameters for both types of Tm noises. The estimation errors of the SDM parameters exhibit large variations. This is mainly caused by the poor estimation performance of I_o (detailed in Section F of SI, also observable from Fig. 8 and Table 2). Globally, the relative RMSE and r^2 score are less impacted by random noise of T_m but increase when large systematic measurement errors are introduced into the input data. Notably, the degradation rate errors of the parameters on average are relatively stable to both types of T_m noise, especially the *I-V* parameter estimations.

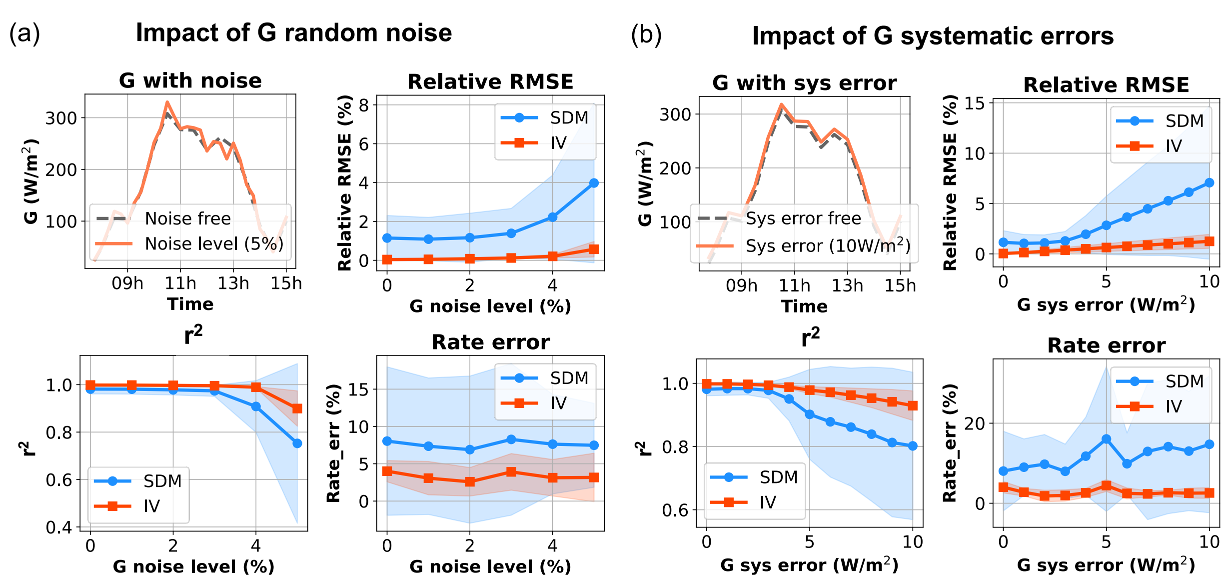

Fig. 10 (a) Example of irradiance (G) with random noise and the three metrics of estimated SDM and *I-V* parameters with G under different random noise levels. The noise level refers to the variance of the normal distribution added to the G. (b) Example of G with systematic error and the three metrics of estimated SDM and *I-V* parameters with G under different systematic error levels. The dotted lines refer to the mean value of all the five SDM or five *I-V* parameter errors, while the filled area outlines the standard deviation of the parameter errors.

It is observed from Fig. 10 that the RMSE and r^2 score of *I-V* and SDM parameters all increase with the random noise or systematic error of G. Similar to the results from Fig. 9, the estimation performance of *I-V* parameters is better than that of SDM parameters. Overall, the degradation rate error of *I-V* and SDM parameters on average is relatively insensitive to both noise types of G, which demonstrates the robustness of PVPRO on the estimated degradation rate.

3.3 Impact of the presence of faults

In addition to measurement noise or errors, various faults may occur in fielded PV modules, causing changes in module performance and the corresponding SDM parameters. In this section, we add some sudden changes to specific parameters to simulate the occurrence of faults in the PV array and evaluate PVPRO under these conditions. We select two SDM parameters (I_{ph_ref} and R_{s_ref}) for study. A decrease is set for I_{ph_ref}, which is usually caused by shading (Pachauri et al., 2020) or soiling (Qasem et al., 2014). For R_{s_ref}, an increase is set, which is generally due to the solder band failure (Asadpour et al., 2020). To approximate the field measurement, a certain amount of measurement noise is also added to *G* and *Tm* (*G*: 2% random noise level, 3W/m^2 systematic error; *Tm*: 1% random noise level, 0.5°C systematic error).

The severity of the fault depends on the duration or magnitudes of change. Here, we addressed four patterns of change with different duration or magnitudes, as detailed in Table 3. The duration of the fault is set as multiples of the time window. When the duration is shorter than the window length, PVPRO will average the results or identify them as outliers. Therefore, PVPRO is tested for detecting anomalies with longer duration than the time window. If the user wants to track anomalies of short durations, the length of the analysis time window should be correspondingly adjusted.

Table 3 Definition of the four cases of fault with different duration and magnitude

	Duration	**Magnitude**
Case short-small	Short (1x time window)*	Small (5%)◊
Case short-large	Short (1x time window)	Large (25%)
Case long-small	Long (10x time window)	Small (5%)
Case long-large	Long (10x time window)	Large (25%)

* The duration of fault is synchronized with the time window for analysis (here, 1 time window = 2 weeks)
◊ The magnitude is a relative value based on the initial value of the parameter

To illustrate this procedure, the evolution trends of the parameters estimated by PVPRO when I_{ph_ref} presents an abnormal decrease under the case short-small (defined in Table 3) are presented in Fig. 11.

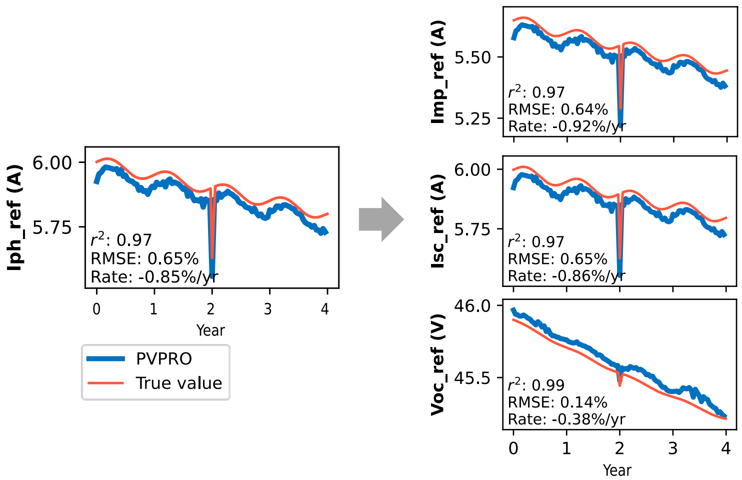

Fig. 11 Estimated parameters when I_{ph} decreases due to a modeled fault. The decrease of I_{ph} is reflected in the change of I_{sc}, I_{mp}, and V_{oc}.

It is observed in Fig. 11 that there is a nearly constant shift between the PVPRO results and the true value, which is primarily due to the measurement error added on *G* and *Tm*. Despite this error, PVPRO can closely capture the sudden decrease of I_{ph_ref} with a relative RMSE of 0.65% and the r^2 score of 0.97. Furthermore, when I_{ph_ref} decreases, the related *I-V* parameters (I_{sc_ref}, I_{mp_ref}, and V_{oc_ref}) will also correspondingly change, as seen from the curves of true values in Fig. 11. For these parameters, the abnormal change is also well captured by PVPRO.

The other patterns of change listed in Table 3 are also tested with the results presented and compared in Fig. 12.

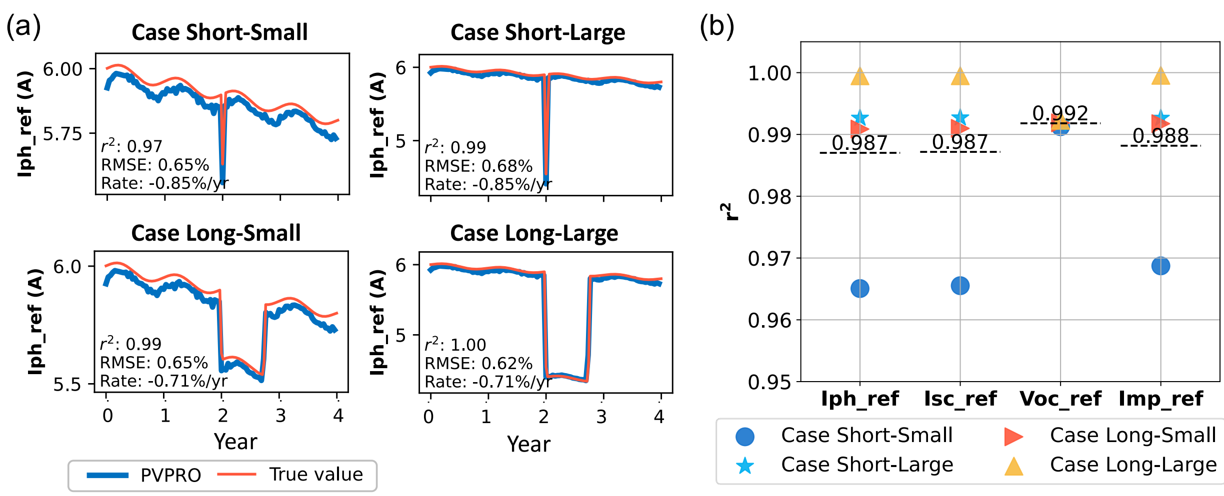

Fig. 12 (a) Four cases of I_{ph} decreases, (b) r^2 of parameters under the four cases. We can observe that the estimated parameters catch well all the cases of change with the r^2 score larger than 0.99.

It is depicted in Fig. 12 that all the cases of I_{ph_ref} change are well captured by PVPRO with an r^2 score >0.97. Among the I_{ph_ref}-impacted parameters, the performance of I_{sc_ref} and I_{mp_ref} are better than that of V_{oc_ref} since they are all the current-related parameters and thus more sensitive to the change of I_{ph_ref}. Under all the cases, the parameters estimated by PVPRO present a near perfect match to the true trend with the average r^2 score higher than 0.98.

Similar studies are performed for R_{s_ref} with the results shown in Fig. 13 and Fig. 14. Regarding the change of R_{s_ref}, V_{mp_ref} and P_{mp_ref} are the affected parameters as presented in Fig. 13.

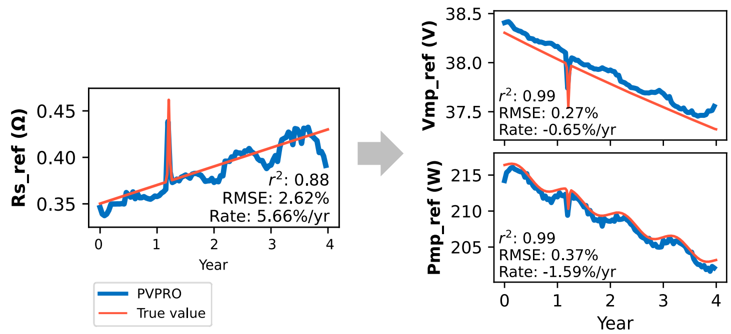

Fig. 13 Estimated parameters when R_{s_ref} increases. The increase of R_{s_ref} causes the change of V_{mp_ref} and P_{mp_ref}.

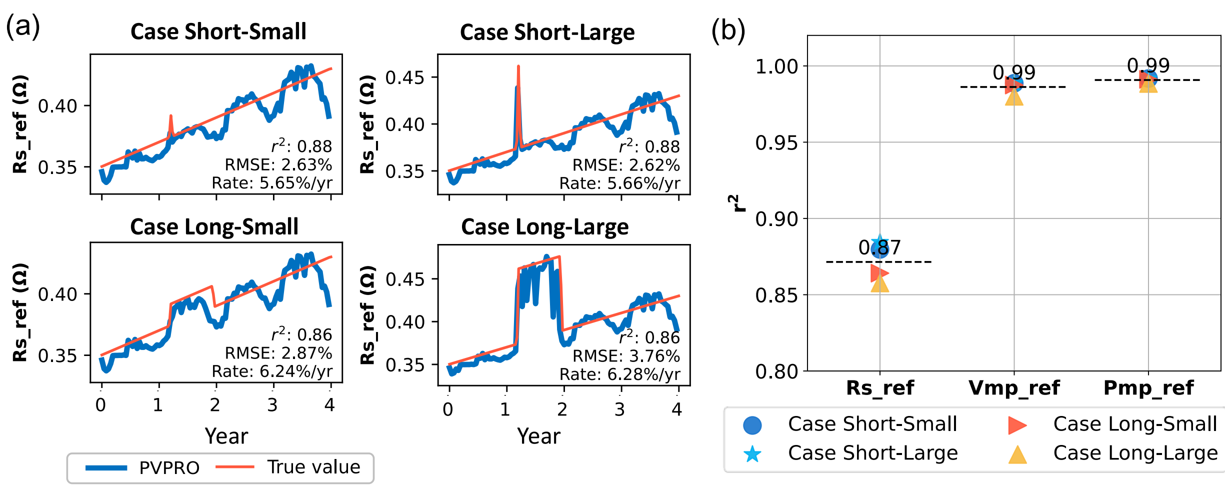

Fig. 14 (a) Four cases of R_{s_ref} increases, (b) r^2 of parameters under the four cases. It is shown that estimated R_{s_ref} could substantially catch the sudden jumps but with oscillation and a better estimation is achieved for V_{mp_ref} and I_{mp_ref}.

Given Fig. 13 and Fig. 14, it is noticed that the r^2 values are relatively independent of fault duration or magnitude. Similar to the previous results in Fig. 8, oscillations occur in the estimated R_{s_ref} trend, which lowers the r^2 score. Nevertheless, the related *I-V* parameters (V_{mp_ref} and I_{mp_ref}) can still be well estimated with the r^2 score higher than 0.99. In short, all the cases of the increasing R_{s_ref} could be well captured by PVPRO with the average r^2 score higher than 0.87 in the presence of noise.

The results of this study of temporary R_{s_ref} increase demonstrate an exciting possibility for on-line maintenance. PV connector fires can occur if the PV connector develops high resistance due to improper construction or installation (PVEL, 2022). Therefore, with further improvements to data quality, PVPRO has the potential to detect incipient failures of the PV connector.

4 Demonstration with field datasets

To evaluate the in-field performance of PVPRO, the NIST-ground array dataset (Boyd et al., 2017) is selected. The PV array is located in Gaithersburg, Maryland, USA (39°07'54.8"N 77°12'52.5"W), is ground mounted and has a fixed tilt angle of 20° (Fig. 15). A total of 1152 modules (Sharp NU-U235F2, 235W, sc-Si) are installed in this array, yielding 271 kW output. The operation and environmental data are continuously recorded with a time step of 1 minute with the data from 2015 to 2019 available for analysis. The output DC power of the array over time is plotted in Fig. 16. The plane-of-array irradiance is measured by a reference cell and the module temperature by a probe attached to the back sheet of the PV module. Besides, a weather station is also configured to measure meteorological data like diffuse/global horizontal irradiance, wind speed, and ambient temperature.

Fig. 15 NIST-ground array with 1152 PV modules yielding 271 kW. The operation and environmental data from this array are used to evaluate PVPRO.

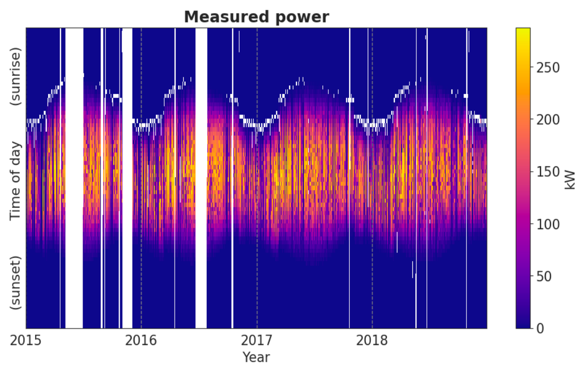

Fig. 16 Heatmap of the output DC power of the PV array from 2015-2019. Invalid data are presented in white.

PVPRO is applied to this dataset following the pipeline presented in Fig. 1. The identified operation condition of the PV array over time is presented in Fig. 2. To validate the modeling performance of PVPRO, the measured operation data (V_{DC} and I_{DC}) are compared with the ones modeled at the measured environmental condition using the SDM parameters estimated by PVPRO. An example of the comparison is depicted in Fig. 17.

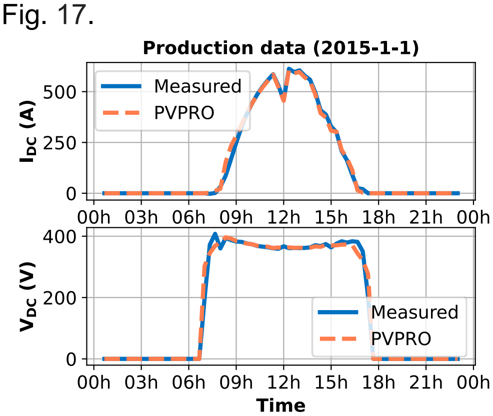

Fig. 17 Comparison of the estimated and measured PV array production data on 2015-1-1. It is shown that the estimated V_{DC} and I_{DC} using PVPRO match the measured ones.

It is shown in Fig. 17 that the estimated V_{DC} and I_{DC} show a good match with the measured ones. For all the operation data from 2015-2019, the average relative error of V_{DC} and I_{DC} is under 1%, which validates the SDM used in PVPRO for the parameter estimation and modeling.

The time-evolution trends of the *I-V* and SDM parameters extracted by PVPRO are presented in Fig. 18. The YOY trend is calculated based on the energy composition of time-series data with a 90% Monte Carlo-derived confidence interval by adopting the Rdtools function (Jordan et al., 2018). It should be noted that an accurate ground truth of these parameters under STC for the array is difficult to obtain. Thus, a quantifiable evaluation of the estimation performance is not performed in this case study; rather, we can conclude that the SDM parameters fit by PVPRO are consistent with the measured V_{DC} and I_{DC}.

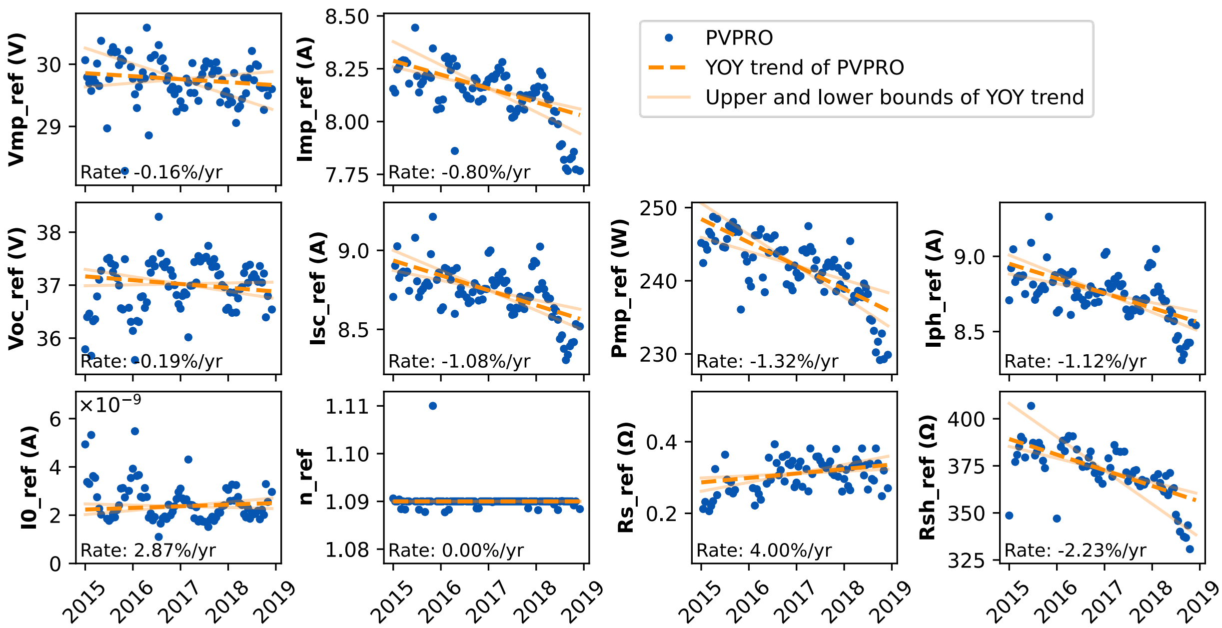

Fig. 18 Estimated parameters using NIST-ground dataset. The upper and lower bounds of the YOY trend are based on the 90% confidence level. All parameters show a degradation over time with some parameters exhibiting a seasonal variation. A sharp decrease in the final year for the current-related parameters is identified. These results extracted by PVPRO may potentially be helpful for the O&M of this PV system.

As plotted in Fig. 18, reasonable degradation trends are observed for all the estimated parameters. The 1.3%/year degradation of P_{mp_ref} is revealed to be mainly due to the degradation of I_{ph} at 1.1%/year, which also similarly impacts the I_{mp_ref} and I_{sc_ref}. The seasonality (the yearly-repeated difference between summer and winter time (Victoria et al., 2021)) is identified for parameters like V_{mp_ref}, V_{oc_ref}, and I_{mp_ref}. For V_{mp_ref} and V_{oc_ref}, the degradation rate is mild, with the magnitude of YOY rate of change < 0.2%/year. Regarding R_{s_ref} and R_{sh_ref}, the rates fall within the common range reported in the literature (Aghaei et al., 2022; Kahoul et al., 2021). As for current-related parameters (I_{mp_ref}, I_{sc_ref}, I_{ph_ref}, and V_{mp_ref}), the rate is moderate, around 1%/year. However, it is noteworthy that a similar sharp decrease occurs in the final year of measurement for these parameters, which is also observed for R_{sh_ref}. This is potentially due to accelerated accumulation of crystal defects in the PV cell leading to a quickly degraded R_{sh_ref}. It will require further effort and perhaps more detailed characterization of the NIST ground array modules to further trace the root cause.

To conclude, the modeling performance of PVPRO is validated on the field PV operation data. PVPRO can extract the time-evolution trends of both SDM and *I-V* parameters. This allows the analysis of the degradation pattern and the identification of the abnormal parameters, which will substantially facilitate the root cause tracking and effective O&M planning for PV systems.

5 Discussion

PVPRO estimates the five SDM parameters by minimizing the errors of two parameters (operation voltage and current) at a variety of temperature and irradiance conditions. Thus, this fitting process may not always guarantee a good estimation of all the five parameters simultaneously, as observed from the oscillation of R_{s_ref} and R_{sh_ref}. More sophisticated fitting techniques may be applied in the future considering the prior probabilities for the variation of parameters and the fitting order of the five SDM parameters. Furthermore, more investigation may be needed into cases where the SDM is not a good match to the system, *e.g.,* as in the case of cell mismatch, and whether such conditions can be detected by PVPRO.

It should be noted that the degradation of a PV array on the order of ~1%/year is similar to the uncertainties with which many parameters can be measured over one year. For example, these uncertainties can be from the infrequent cleaning of the pyranometer or reference cell and the measurement error of the operating voltage and current. However, the error of measurement devices is typically expected to be constant with time, or slowly changing with time bounded to under a few percent. Therefore, the analysis of longer-term data sets can be made with higher confidence for PVPRO. In addition, the quality of the available field data is also essential to the PVPRO's performance. Thus, for the field application, the readings and drift magnitude from multiple sensors in a PV array should be validated and the cases like sensors are swapped for maintenance or calibration should be also well handled.

Finally, PVPRO is published as an open-source Python package (https://github.com/DuraMAT/pvpro), which may be integrated with other common PV analysis packages (*e.g.*, pvlib (Holmgren et al., 2018), solar-data-tools (Meyers et al., 2022)) for further customization.

6 Conclusion

This paper proposes a methodology (PVPRO) for estimating the PV circuit model parameters from routine PV operation data. On synthetic datasets, PVPRO achieves an excellent estimation of both the single-diode model (SDM) and the *I-V* parameters (open-circuit voltage, short-circuit current, maximum power, etc.) with an average error of 0.55%. Degradation trends are also accurately identified with a coefficient of determination (r^2) of 0.99. Notably, the estimated degradation rate of parameters, especially for the *I-V* parameters, is generally robust to the varying random or systematic measurement noise. In the presence of faults on SDM parameters, PVPRO can also closely capture the trends with r^2 higher than 0.86. In addition, PVPRO is evaluated on a field PV dataset (271kW PV array). The modeling performance is validated with errors less than 1% between the measured and estimated operation data for the directly fitted quantities, although validation of extracted SDM parameters was not possible in this study. The extracted degradation trends of the SDM and *I-V* parameters effectively facilitate the identification of abnormal parameters and tracing root causes for PV operation and maintenance. PVPRO is published as an open-source Python package (https://github.com/DuraMAT/pvpro). Future work aims to further evaluate PVPRO on more large-scale field PV datasets closer to production environments.

7 Acknowledgment

The authors would like to thank Muhammad Ashraful Alam and Laura Schelhas for the insightful discussions. They would also like to thank Stephanie Moffitt for providing updated information on the NIST dataset. The project was primarily funded and intellectually led as part of the Durable Modules Consortium (DuraMAT), an Energy Materials Network Consortium funded under Agreement 32509 by the U.S. Department of Energy (DOE), Office of Energy Efficiency & Renewable Energy, Solar Energy Technologies Office (EERE, SETO). Lawrence Berkeley National Laboratory is funded by the DOE under award DE-AC02-05CH11231.This work was authored in part by the National Renewable Energy Laboratory, operated by Alliance for Sustainable Energy, LLC, for the U.S. Department of Energy (DOE) under Contract No. DE-AC36-08GO28308. The views expressed in the article do not necessarily represent the views of the DOE or the U.S. Government. The U.S. Government retains and the publisher, by accepting the article for publication, acknowledges that the U.S. Government retains a nonexclusive, paid-up, irrevocable, worldwide license to publish or reproduce the published form of this work, or allow others to do so, for U.S. Government purposes.

8 References

Aghaei, M., Fairbrother, A., Gok, A., Ahmad, S., Kazim, S., Lobato, K., Oreski, G., Reinders, A., Schmitz, J., Theelen, M., Yilmaz, P., Kettle, J., 2022. Review of degradation and failure phenomena in photovoltaic modules. Renewable and Sustainable Energy Reviews 159, 112160. https://doi.org/10.1016/J.RSER.2022.112160

Alam, M.K., Khan, F., Johnson, J., Flicker, J., 2015. A Comprehensive Review of Catastrophic Faults in PV Arrays: Types, Detection, and Mitigation Techniques. IEEE J Photovolt 5, 982–997. https://doi.org/10.1109/JPHOTOV.2015.2397599

Alia-Martinez, M., Antonanzas, J., Urraca, R., Martinez-De-Pison, F.J., Antonanzas-Torres, F., 2016. Benchmark of algorithms for solar clear-sky detection. Journal of Renewable and Sustainable Energy 8, 033703. https://doi.org/10.1063/1.4950948

Allen-Zhu, Z., Li, Y., Song, Z., 2018. A Convergence Theory for Deep Learning via Over-Parameterization. 36th International Conference on Machine Learning, ICML 2019 2019-June, 362–372. https://doi.org/10.48550/arxiv.1811.03962

Asadpour, R., A. Alam, M., 2022. Worldwide Lifetime Prediction of c-Si Modules Due to Finger Corrosion: A Phenomenological Approach. IEEE J Photovolt.

Asadpour, R., Patel, M.T., Clark, S., Alam, M.A., 2021. Worldwide Physics-Based Analysis of Solder Bond Failure in c-Si Modules for Lifetime Prediction. Conference Record of the IEEE Photovoltaic Specialists Conference 260–263. https://doi.org/10.1109/PVSC43889.2021.9518931

Asadpour, R., Sulas-Kern, D.B., Johnston, S., Meydbray, J., Alam, M.A., 2020. Dark lock-in thermography identifies solder bond failure as the root cause of series resistance increase in fielded solar modules. IEEE J Photovolt 10, 1409–1416. https://doi.org/10.1109/JPHOTOV.2020.3003781

Batzelis, E., 2019. Non-Iterative Methods for the Extraction of the Single-Diode Model Parameters of Photovoltaic Modules: A Review and Comparative Assessment. Energies 2019, Vol. 12, Page 358 12, 358. https://doi.org/10.3390/EN12030358

Boyd, M., Chen, T., Dougherty, B., 2017. NIST Campus Photovoltaic (PV) Arrays and Weather Station Data Sets [WWW Document]. National Institute of Standards and Technology. U.S. Department of Commerce, Washington, D.C. [Data set]. URL https://doi.org/10.18434/M3S67G (accessed 5.19.22).

Cardenas, A.A., Carrasco, M., Mancilla-David, F., Street, A., Cardenas, R., 2017. Experimental Parameter Extraction in the Single-Diode Photovoltaic Model via a Reduced-Space Search.

IEEE Transactions on Industrial Electronics 64, 1468–1476. https://doi.org/10.1109/TIE.2016.2615590

Chakar, J., Pavlov, M., Bonnassieux, Y., Badosa, J., 2022. Determining solar cell parameters and degradation rates from power production data. Energy Conversion and Management: X 15, 100270. https://doi.org/10.1016/J.ECMX.2022.100270

Chen, X., Karin, T., Jain, A., 2022. Automated defect identification in electroluminescence images of solar modules. Solar Energy 242, 20–29. https://doi.org/10.1016/J.SOLENER.2022.06.031

David, T.W., Soares, G.A., Bristow, N., Bagnis, D., Kettle, J., 2021. Predicting diurnal outdoor performance and degradation of organic photovoltaics via machine learning; relating degradation to outdoor stress conditions. Progress in Photovoltaics: Research and Applications 29, 1274–1284. https://doi.org/10.1002/PIP.3453

De Blas, M.A., Torres, J.L., Prieto, E., García, A., 2002. Selecting a suitable model for characterizing photovoltaic devices. Renew Energy 25, 371–380. https://doi.org/10.1016/S0960-1481(01)00056-8

De la Parra, I., Muñoz, M., Lorenzo, E., García, M., Marcos, J., Martínez-Moreno, F., 2017. PV performance modelling: A review in the light of quality assurance for large PV plants. Renewable and Sustainable Energy Reviews 78, 780–797. https://doi.org/10.1016/J.RSER.2017.04.080

De Soto, W., Klein, S.A., Beckman, W.A., 2006. Improvement and validation of a model for photovoltaic array performance. Solar Energy 80, 78–88. https://doi.org/10.1016/J.SOLENER.2005.06.010

Dirnberger, D., Kraling, U., 2013. Uncertainty in PV module measurement-part I: Calibration of crystalline and thin-film modules. IEEE J Photovolt 3, 1016–1026. https://doi.org/10.1109/JPHOTOV.2013.2260595

D.L. King, W.E. Boyson, J.A. Kratochvill, 2004. Photovoltaic Array Performance Model [WWW Document]. SAND2004-3535 Report. URL https://www.osti.gov/servlets/purl/919131 (accessed 8.5.22).

Dobos, A.P., 2012. An improved coefficient calculator for the california energy commission 6 parameter photovoltaic module model. Journal of Solar Energy Engineering, Transactions of the ASME 134. https://doi.org/10.1115/1.4005759/455696

Doll, B., Hepp, J., Hoffmann, M., Schuler, R., Buerhop-Lutz, C., Peters, I.M., Hauch, J.A., Maier, A., Brabec, C.J., 2021. Photoluminescence for Defect Detection on Full-Sized Photovoltaic Modules. IEEE J Photovolt 11, 1419–1429. https://doi.org/10.1109/JPHOTOV.2021.3099739

Friesen, G., Herrmann, W., Belluardo, G., Herteleer, B., 2018. Report IEA-PVPS T13-11:2018 Photovoltaic module energy yield measurements: Existing approaches and best practice, IEA-PVPS.

Holmgren, W.F., Hansen, C.W., Mikofski, M.A., 2018. pvlib python: a python package for modeling solar energy systems. J Open Source Softw 3, 884. https://doi.org/10.21105/JOSS.00884

Humada, A.M., Darweesh, S.Y., Mohammed, K.G., Kamil, M., Mohammed, S.F., Kasim, N.K., Tahseen, T.A., Awad, O.I., Mekhilef, S., 2020. Modeling of PV system and parameter extraction based on experimental data: Review and investigation. Solar Energy 199, 742–760. https://doi.org/10.1016/J.SOLENER.2020.02.068

Humada, A.M., Hojabri, M., Mekhilef, S., Hamada, H.M., 2016. Solar cell parameters extraction based on single and double-diode models: A review. Renewable and Sustainable Energy Reviews 56, 494–509. https://doi.org/10.1016/J.RSER.2015.11.051

IEA, 2021. Net Zero by 2050 A Roadmap for the Global Energy Sector.

Ineichen, P., 2016. Validation of models that estimate the clear sky global and beam solar irradiance. Solar Energy 132, 332–344. https://doi.org/10.1016/J.SOLENER.2016.03.017

Jahn, U., Herz, M., Köntges, M., Parlevliet, D., Paggi, M., Tsanakas, I., 2018. Report IEA-PVPS T13-10:2018- Review on Infrared and Electroluminescence Imaging for PV Field Applications. International Energy Agency.

Jones, C.B., Hansen, C.W., 2019. Single Diode Parameter Extraction from In-Field Photovoltaic I-V Curves on a Single Board Computer. Conference Record of the IEEE Photovoltaic Specialists Conference 382–387. https://doi.org/10.1109/PVSC40753.2019.8981330

Jordan, D.C., Deline, C., Kurtz, S.R., Kimball, G.M., Anderson, M., 2018. Robust PV Degradation Methodology and Application. IEEE J Photovolt 8, 525–531. https://doi.org/10.1109/JPHOTOV.2017.2779779

Jordan, D.C., Kurtz, S.R., 2014. The dark horse of evaluating long-term field performance-Data filtering. IEEE J Photovolt 4, 317–323. https://doi.org/10.1109/JPHOTOV.2013.2282741

Jordan, D.C., Kurtz, S.R., 2013. Photovoltaic Degradation Rates—an Analytical Review. Progress in Photovoltaics: Research and Applications 21, 12–29. https://doi.org/10.1002/PIP.1182

Kahoul, N., Cheghib, H., Sidrach-de-Cardona, M., Affari, B.C., Younes, M., Kherici, Z., 2021. Performance degradation analysis of crystalline silicon solar cells in desert climates. Energy for Sustainable Development 65, 189–193. https://doi.org/10.1016/J.ESD.2021.10.010

Kalliojärvi, H., Lappalainen, K., Valkealahti, S., 2022. Feasibility of Photovoltaic Module Single-Diode Model Fitting to the Current–Voltage Curves Measured in the Vicinity of the Maximum Power Point for Online Condition Monitoring Purposes. Energies 2022, Vol. 15, Page 9079 15, 9079. https://doi.org/10.3390/EN15239079

Kalliojärvi-Viljakainen, H., Lappalainen, K., Valkealahti, S., 2022. A novel procedure for identifying the parameters of the single-diode model and the operating conditions of a photovoltaic module from measured current–voltage curves. Energy Reports 8, 4633–4640. https://doi.org/10.1016/J.EGYR.2022.03.141

Killam, A.C., Karas, J.F., Augusto, A., Bowden, S.G., 2021. Monitoring of Photovoltaic System Performance Using Outdoor Suns-VOC. Joule 5, 210–227. https://doi.org/10.1016/J.JOULE.2020.11.007

Kumar, M., Kumar, A., 2017. Performance assessment and degradation analysis of solar photovoltaic technologies: A review. Renewable and Sustainable Energy Reviews 78, 554–587. https://doi.org/10.1016/J.RSER.2017.04.083

Lappalainen, K., Manganiello, P., Piliougine, M., Spagnuolo, G., Valkealahti, S., 2020. Virtual Sensing of Photovoltaic Module Operating Parameters. IEEE J Photovolt 10, 852–862. https://doi.org/10.1109/JPHOTOV.2020.2972688

Lappalainen, K., Piliougine, M., Spagnuolo, G., 2022. Experimental comparison between various fitting approaches based on RMSE minimization for photovoltaic module parametric identification. Energy Convers Manag 258, 115526. https://doi.org/10.1016/J.ENCONMAN.2022.115526

Li, B., Delpha, C., Migan-Dubois, A., Diallo, D., 2021a. Fault diagnosis of photovoltaic panels using full I–V characteristics and machine learning techniques. Energy Convers Manag 248, 114785. https://doi.org/10.1016/J.ENCONMAN.2021.114785

Li, B., Diallo, D., Migan-Dubois, A., Delpha, C., 2022. Performance evaluation of IEC 60891:2021 procedures for correcting I–V curves of photovoltaic modules under healthy and faulty conditions. Progress in Photovoltaics: Research and Applications. https://doi.org/10.1002/PIP.3652

Li, B., Migan-Dubois, A., Delpha, C., Diallo, D., 2021b. Evaluation and improvement of IEC 60891 correction methods for I-V curves of defective photovoltaic panels. Solar Energy 216, 225–237. https://doi.org/10.1016/j.solener.2021.01.010

Li, G., Duan, Z., Liang, L., Zhu, H., Hu, A., Cui, Q., Chen, B., Hu, W., 2020. Outlier data mining method considering the output distribution characteristics for photovoltaic arrays and its application. Energy Reports 6, 2345–2357. https://doi.org/10.1016/J.EGYR.2020.08.034

Lillo-Sánchez, L., López-Lara, G., Vera-Medina, J., Pérez-Aparicio, E., Lillo-Bravo, I., 2021. Degradation analysis of photovoltaic modules after operating for 22 years. A case study with comparisons. Solar Energy 222, 84–94. https://doi.org/10.1016/J.SOLENER.2021.04.026

Lindig, S., Louwen, A., Moser, D., Topic, M., 2020. Outdoor PV System Monitoring—Input Data Quality, Data Imputation and Filtering Approaches. Energies 2020, Vol. 13, Page 5099 13, 5099. https://doi.org/10.3390/EN13195099

Liu, D.C., Nocedal, J., 1989. On the limited memory BFGS method for large scale optimization. Mathematical Programming 1989 45:1 45, 503–528. https://doi.org/10.1007/BF01589116

Livera, A., Theristis, M., Makrides, G., Georghiou, G.E., 2019. Recent advances in failure diagnosis techniques based on performance data analysis for grid-connected photovoltaic systems. Renew Energy 133, 126–143. https://doi.org/10.1016/j.renene.2018.09.101

Mellit, A., Kalogirou, S., 2022. Assessment of machine learning and ensemble methods for fault diagnosis of photovoltaic systems. Renew Energy 184, 1074–1090. https://doi.org/10.1016/J.RENENE.2021.11.125

Mellit, A., Tina, G.M., Kalogirou, S.A., 2018. Fault detection and diagnosis methods for photovoltaic systems: A review. Renewable and Sustainable Energy Reviews 91, 1–17. https://doi.org/10.1016/j.rser.2018.03.062

Meyers, B., Ragsdale, D., Serbetcioglu, D., Goncalves, J., alejandro350, tadatoshi, Apostolaki, E., Rodriguez, D.J.F., 2022. solar-data-tools: v0.7.0 [WWW Document]. Zenodo. https://doi.org/10.5281/ZENODO.6964919

Meyers, B., Tabone, M., Kara, E.C., 2019. Statistical Clear Sky Fitting Algorithm. https://doi.org/10.48550/arxiv.1907.08279

Meyers, B.E., Apostolaki-Iosifidou, E., Schelhas, L.T., 2020. Solar Data Tools: Automatic Solar Data Processing Pipeline. Conference Record of the IEEE Photovoltaic Specialists Conference 2020-June, 0655–0656. https://doi.org/10.1109/PVSC45281.2020.9300847

MorganSolar, 2022. IV DAQ & Analytics Portal [WWW Document]. URL https://morgansolar.com/daq (accessed 9.12.22).

Ndiaye, A., Charki, A., Kobi, A., Kébé, C.M.F., Ndiaye, P.A., Sambou, V., 2013. Degradations of silicon photovoltaic modules: A literature review. Solar Energy 96, 140–151. https://doi.org/10.1016/J.SOLENER.2013.07.005

Pachauri, R.K., Mahela, O.P., Sharma, A., Bai, J., Chauhan, Y.K., Khan, B., Alhelou, H.H., 2020. Impact of partial shading on various PV array configurations and different modeling approaches: A comprehensive review. IEEE Access 8, 181375–181403. https://doi.org/10.1109/ACCESS.2020.3028473

Padmavathi, K., Daniel, S.A., 2013. Performance analysis of a 3 MWp grid connected solar photovoltaic power plant in India. Energy for Sustainable Development 17, 615–625. https://doi.org/10.1016/J.ESD.2013.09.002

Phinikarides, A., Kindyni, N., Makrides, G., Georghiou, G.E., 2014. Review of photovoltaic degradation rate methodologies. Renewable and Sustainable Energy Reviews 40, 143–152. https://doi.org/10.1016/j.rser.2014.07.155

Pillai, D.S., Rajasekar, N., 2018. A comprehensive review on protection challenges and fault diagnosis in PV systems. Renewable and Sustainable Energy Reviews 91, 18–40. https://doi.org/10.1016/j.rser.2018.03.082

PVEL, 2022. The Ultimate Safety Guide for Solar PV Connectors.

Qasem, H., Betts, T.R., Müllejans, H., Albusairi, H., Gottschalg, R., 2014. Dust-induced shading on photovoltaic modules. Progress in Photovoltaics: Research and Applications 22, 218–226. https://doi.org/10.1002/PIP.2230

Rahman, M.M., Khan, I., Alameh, K., 2021. Potential measurement techniques for photovoltaic module failure diagnosis: A review. Renewable and Sustainable Energy Reviews 151, 111532. https://doi.org/10.1016/J.RSER.2021.111532

Reise, C., Müller, B., Moser, D., Belluardo, G., Ingenhoven, P., 2018. Report IEA-PVPS T13-12:2018 Uncertainties in PV System Yield Predictions and Assessments.

Schardt, J., te Heesen, H., 2021. Performance of roof-top PV systems in selected European countries from 2012 to 2019. Solar Energy 217, 235–244. https://doi.org/10.1016/J.SOLENER.2021.02.001

SEIA, 2022. Solar Market Insight Report 2021 Year in Review.

Sengupta, M., Xie, Y., Lopez, A., Habte, A., Maclaurin, G., Shelby, J., 2018. The National Solar Radiation Data Base (NSRDB). Renewable and Sustainable Energy Reviews 89, 51–60. https://doi.org/10.1016/J.RSER.2018.03.003

Smirnov, V., Lambertz, A., Böttler, W., Carius, R., Finger, F., Hüpkes, J., v. Smirnov, A. Lambertz, W. Böttler, R. Carius, F.F., 2010. Uncertainty of Field I-V-Curve Measurements in Large Scale PV-Systems. 25th European Photovoltaic Solar Energy Conference and Exhibition / 5th World Conference on Photovoltaic Energy Conversion, 6-10 September 2010, Valencia, Spain 4587–4594. https://doi.org/10.4229/25THEUPVSEC2010-4BV.1.62

Sun, Q., Zhou, W.X., Fan, J., 2020. Adaptive Huber Regression. J Am Stat Assoc 115, 254–265. https://doi.org/10.1080/01621459.2018.1543124/SUPPL_FILE/UASA_A_1543124_SM1170.ZIP

Sun, X., Chavali, R.V.K., Alam, M.A., 2019. Real-time monitoring and diagnosis of photovoltaic system degradation only using maximum power point—the Suns-Vmp method. Progress in Photovoltaics: Research and Applications 27, 55–66. https://doi.org/10.1002/PIP.3043

Tay, S., Lim, I., Ye, Z., Yang, D., Garrigos, A., 2017. PV parameter identification using reduced I-V data. Proceedings IECON 2017 - 43rd Annual Conference of the IEEE Industrial Electronics Society 2017-January, 2653–2657. https://doi.org/10.1109/IECON.2017.8216446

Theristis, M., Livera, A., Jones, C.B., Makrides, G., Georghiou, G.E., Stein, J.S., 2020. Nonlinear Photovoltaic Degradation Rates: Modeling and Comparison against Conventional Methods. IEEE J Photovolt 10, 1112–1118. https://doi.org/10.1109/JPHOTOV.2020.2992432

Toledo, F.J., Blanes, J.M., 2016. Analytical and quasi-explicit four arbitrary point method for extraction of solar cell single-diode model parameters. Renew Energy 92, 346–356. https://doi.org/10.1016/J.RENENE.2016.02.012

Victoria, M., Haegel, N., Peters, I.M., Sinton, R., Jäger-Waldau, A., del Cañizo, C., Breyer, C., Stocks, M., Blakers, A., Kaizuka, I., Komoto, K., Smets, A., 2021. Solar photovoltaics is ready to power a sustainable future. Joule 5, 1041–1056. https://doi.org/10.1016/J.JOULE.2021.03.005

Vuković, M., Jakovljević, M., Flø, A.S., Olsen, E., Burud, I., 2022. Noninvasive photoluminescence imaging of silicon PV modules in daylight. Appl Phys Lett 120, 244102. https://doi.org/10.1063/5.0097576

Wang, M., Liu, J., Burleyson, T.J., Schneller, E.J., Davis, K.O., French, R.H., Braid, J.L., 2020. Analytic Isc-V ocMethod and Power Loss Modes from Outdoor Time-Series I-V Curves. IEEE J Photovolt 10, 1379–1388. https://doi.org/10.1109/JPHOTOV.2020.2993100

Wang, M., Ma, X., Huang, W.H., Liu, J., Curran, A.J., Schnabel, E., Köhl, M., Davis, K.O., Brynjarsdóttir, J., Braid, J.L., French, R.H., 2018. Evaluation of Photovoltaic Module Performance Using Novel Data-driven I-V Feature Extraction and Suns-V OC Determined from Outdoor Time-Series I-V Curves. 2018 IEEE 7th World Conference on Photovoltaic Energy Conversion, WCPEC 2018 - A Joint Conference of 45th IEEE PVSC, 28th PVSEC and 34th EU PVSEC 778–783. https://doi.org/10.1109/PVSC.2018.8547772

Yang, B., Wang, J., Zhang, X., Yu, T., Yao, W., Shu, H., Zeng, F., Sun, L., 2020. Comprehensive overview of meta-heuristic algorithm applications on PV cell parameter identification. Energy Convers Manag 208, 112595. https://doi.org/10.1016/J.ENCONMAN.2020.112595

Zaghba, L., Khennane, M., Mekhilef, S., Fezzani, A., Borni, A., 2022. Experimental outdoor performance assessment and energy efficiency of 11.28 kWp grid tied PV systems with sun tracker installed in saharan climate: A case study in Ghardaia, Algeria. Solar Energy 243, 174–192. https://doi.org/10.1016/J.SOLENER.2022.07.045

Zeb, K., Islam, S.U., Khan, I., Uddin, W., Ishfaq, M., Curi Busarello, T.D., Muyeen, S.M., Ahmad, I., Kim, H.J., 2022. Faults and Fault Ride Through strategies for grid-connected photovoltaic system: A comprehensive review. Renewable and Sustainable Energy Reviews 158, 112125. https://doi.org/10.1016/J.RSER.2022.112125